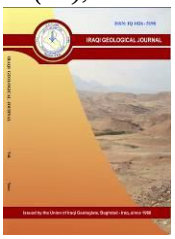
Iraqi Geological Journal

Journal homepage: https://www.igj-iraq.org



Petrophysical Analysis of the Upper Shale Member and the Upper Sand Member of the Zubair Formation in the Zubair Oilfield, Southern Iraq

Rayan H. Al-Atab[1*], Fahad M. Al-Najm[1], and Basim H. Soltan[1]

[1] Department of Geology, College of Science, Basrah University, Basrah, Iraq

[*] **Correspondence**: rayanhassan434@gmail.com

Received:
14 June 2025
Accepted:
3 August 2025
Published:
30 November 2025

Abstract

The Zubair Formation is a major hydrocarbon-bearing unit in southern Iraq, consisting of five distinct members. This study focuses on evaluating the petrophysical properties of its two upper members—the Upper Shale Member and the Upper Sand Member—within the Zubair Oilfield. The objective is to assess the spatial variability and quality of the petrophysical properties across these members using open-hole well log data. Four wells were selected for analysis, each located in a different structural domes: Hammar, Shuaiba, Rafidhiya, and Safwan. Petrophysical analysis was conducted using integrated log interpretation software to calculate key parameters, including shale volume, total porosity, effective porosity, hydrocarbon saturation, bulk volume hydrocarbon, effective bulk volume hydrocarbon, movable oil saturation, and water saturation in the invaded zone (Sxo). Non-reservoir intervals were filtered based on gamma ray values >70 API, porosity <0.05, and hydrocarbon saturation <0.30. The results show that the best petrophysical properties in both members are observed in the Hammar Dome (Z1). In the Upper Shale Member, the poorest properties were recorded in the Shuaiba Dome (Z2). In contrast, the lowest values were observed in the Safwan Dome (Z4) within the Upper Sand Member. An apparent north-to-south decline in petrophysical quality was identified in the Upper Sand Member, but not in the Upper Shale Member. The widespread presence of heavy, tar-like hydrocarbons across all wells may indicate a regional reservoir characteristic. These findings contribute to a better understanding of petrophysical variability in the upper Zubair Formation and can support further geological or reservoir modelling efforts.

Keywords: Southern Iraq; Zubair Oilfield; Zubair Formation; Upper Sand Member; Upper Shale Member; Petrophysical Properties

1. Introduction

The Zubair Formation is one of the most significant Lower Cretaceous reservoirs in Iraq, particularly in the Zubair and Rumaila oilfields, which are classified as major hydrocarbon producers in the region (Jassim and Goff, 2006). It consists mainly of deltaic, fluvio-deltaic, and marine sandstones, spanning a broad area of southern and central Iraq, and extending into northern Saudi Arabia and Kuwait (Powers et al., 1966).

Despite its economic importance, the formation, especially the Upper Shale Member (Z/1) remains under-characterized in terms of spatial petrophysical variability across structural domes within the Zubair Oilfield. Most prior research has focused either on other fields or only on the Upper Sand Member (Z/2). For instance, the reservoir characteristics in the North Rumaila Oilfield. Al-Samer and

Al-Najm (2024) focused on flow units in South Rumaila, and analyzed mineralogical impacts in the Luhais Oilfield.

This study addresses a research gap by evaluating both the Z/1 and Z/2 members within the Zubair Oilfield using data from four productive wells: Z1, Z2, Z3, and Z4, each located in a different domes: Hammar, Shuaiba, Rafidhiya, and Safwan, respectively (Fig.1). The aim is to characterize spatial variability in petrophysical properties using qualitative and quantitative well log analysis. While most productivity studies emphasize the Z/2 Member, this research also considers the Z/1 Member to provide a broader understanding of the reservoir system.

The objective of this study is to assess and compare the petrophysical behavior of the Z/1 and Z/2 members across all four domes to support future hydrocarbon development and enhanced reservoir management.

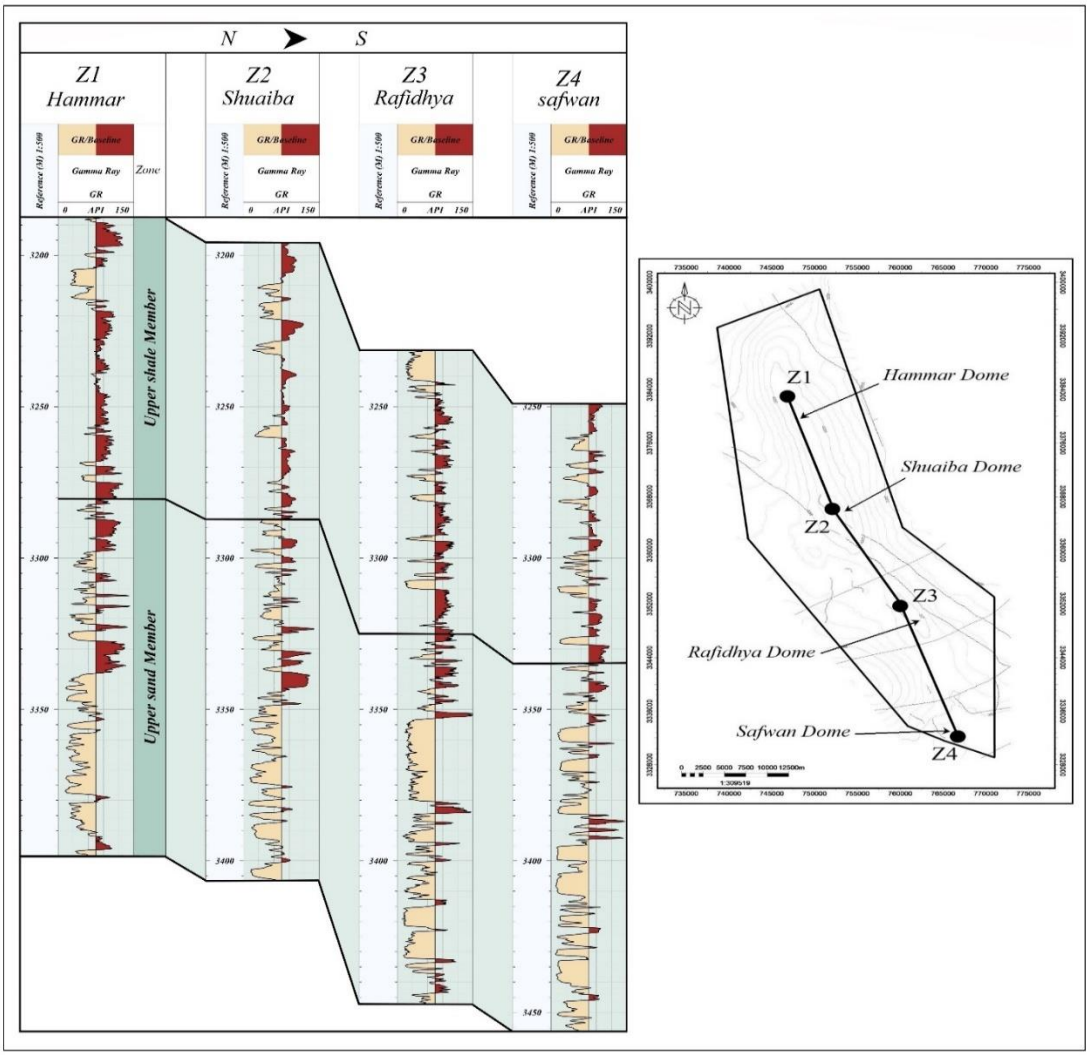


Fig.1. North–south correlation of Z/1 and Z/2 members in the Zubair Oilfield using gamma ray logs from wells Z1 (Hammar), Z2 (Shuaiba), Z3 (Rafidhya), and Z4 (Safwan)

2. Study Area

The Zubair Oilfield is located about 20 km west of Basrah City in southern Iraq, between longitudes 47°32′E and 47°45′E and latitudes 30°05′N and 30°42′N (Fig. 2). It extends approximately 67 km in length and 8.7 km in width, giving a length-to-width ratio of 7.7, which classifies it as a linear fold (Al-Mutury and Al-Mayahi, 2010). The field is part of a prolific hydrocarbon-bearing region in

southern Iraq and has been extensively developed for oil production over several decades. Its structural configuration plays a key role in hydrocarbon accumulation, making it a significant focus for petrophysical and geological studies.

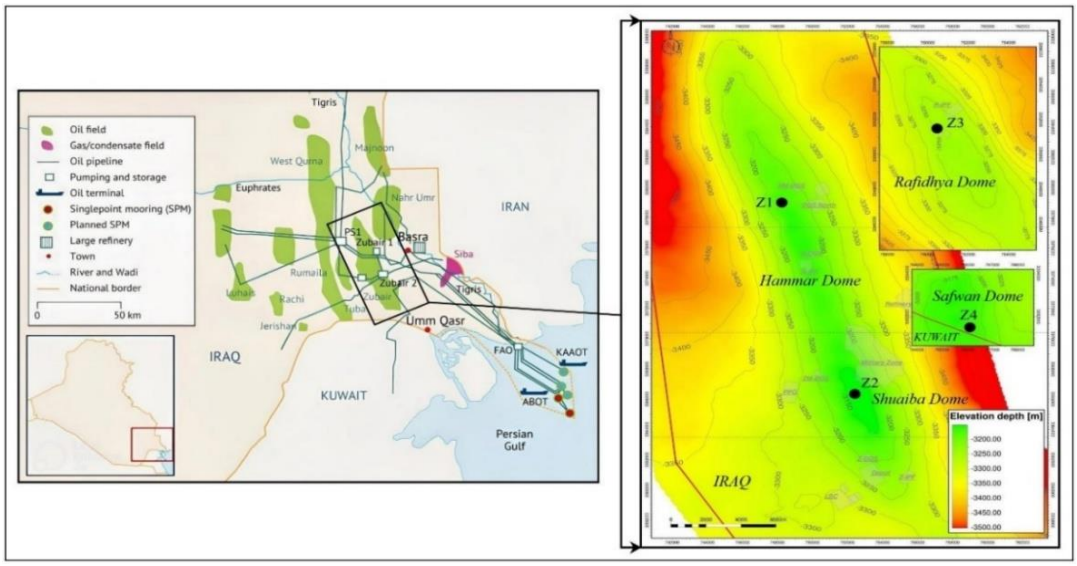


Fig. 2. a) Map showing major oilfields in southern Iraq, with the Zubair Oilfield highlighted by a black square (adapted from Alher et al., 2018), and b) Structural contour map showing depth variations and locations of the four study wells

3. Geological Setting

The Mesopotamian Zone comprises the Tigris, Euphrates, and Zubair subzones and is part of the Unstable Outer Platform of the Arabian Plate. The Zubair subzone, situated in southeastern Iraq, is bounded to the north by the Takhadid-Qurna transversal fault, while its southern boundary is delineated by the Al-Batin fault or a transversal fault in Kuwait (Fig.3).

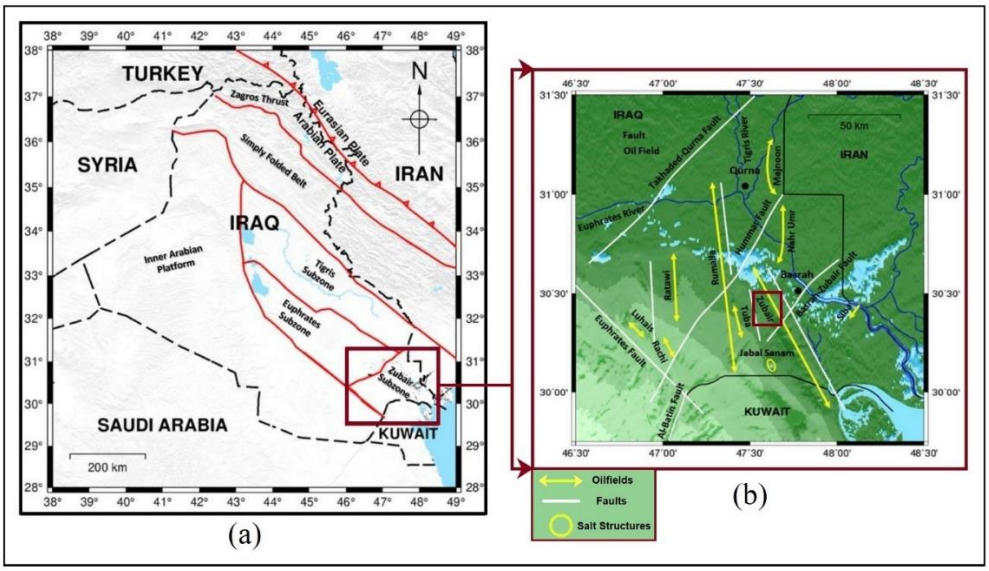


Fig. 3. a) The tectonic framework of Iraq and the detailed subdivisions within the Mesopotamian Zone (Buday and Jassim, 1987; Jassim and Goff, 2006), and b) Illustration of subsurface anticlines (oilfields), fault systems, and salt structures within the Zubair subzone adapted from SOC (1986) and Al-Najar (1989), according to Abdulnaby (2018)

The Zubair subzone developed within a shallow marine environment, influenced by tectonic activity that caused fluctuating sea levels and led to repeated cycles of regression and transgression. This subzone exhibits multiple depositional cycles, each separated by intervals of non-deposition and erosion (Numan, 2000; Mahdi and Mustafa, 2018). The Zubair Formation was deposited during a sea-level lowstand and is characterized by the Barremian–Aptian sequence, belonging to the Thamama Group (Fig. 4). Along with the Upper Tithonian–Aptian Thamama Group and the Albian–Turonian Wasi'a Group, it forms the AP8 megasequence (Jassim and Goff, 2006).

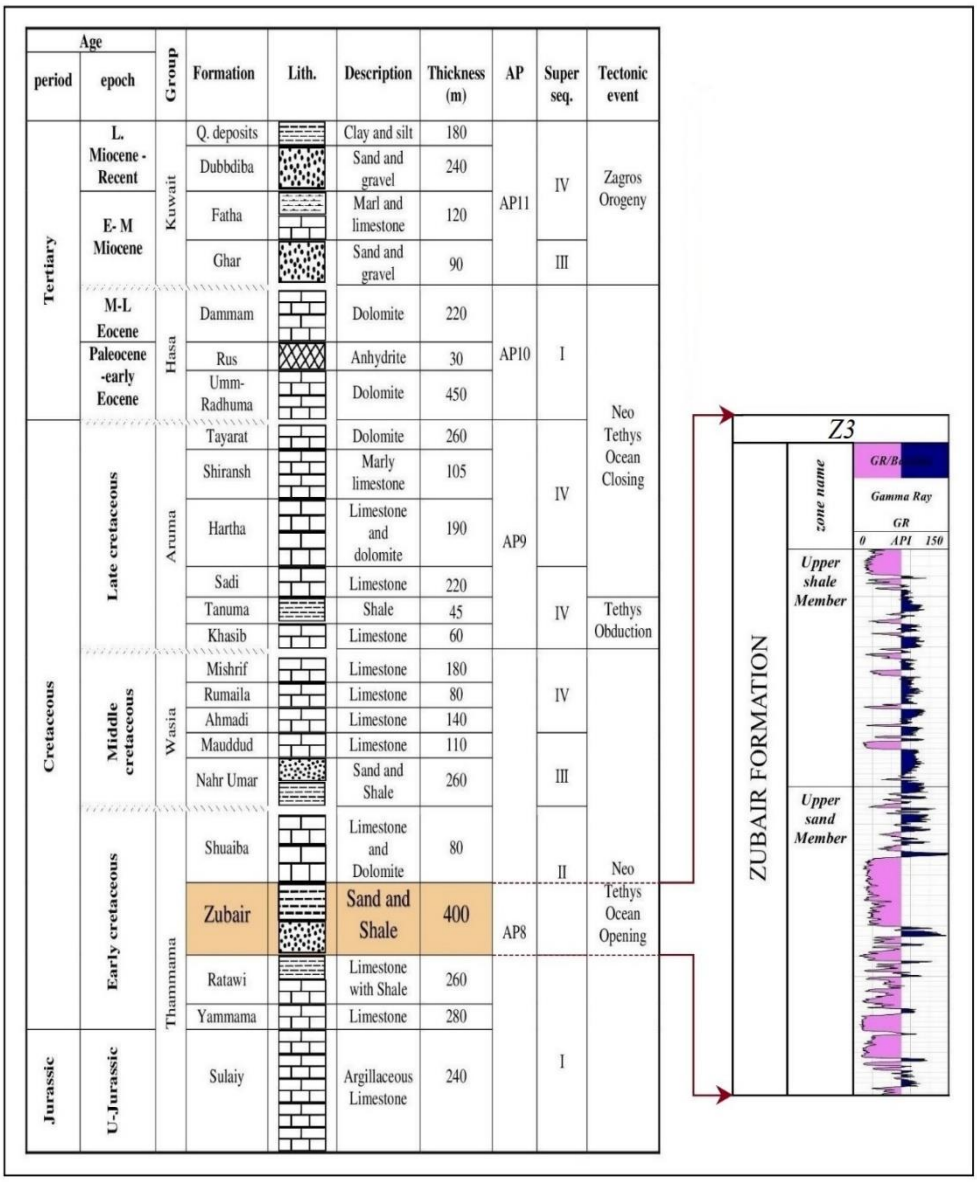


Fig. 4. The stratigraphic column for the Zubair Oilfield, adapted from Sharland et al. (2001) and Aqrawi et al. (2010)

Structurally, the Zubair subzone is distinguished by numerous elongated folds oriented north-south to northwest-southeast, which host several major oilfields. These Late Cretaceous folds are primarily linear, narrow anticlines. Two main subsurface structural types form the basis of oilfields in this subzone: folds and salt domes. The Zubair Oilfield is classified as a folded structure (Jassim and Goff, 2006).

The Zubair Oilfield itself comprises four domes: Hammar, Shuaiba, Rafidhya, and Safwan. These domes display an asymmetrical fold pattern, with the western limbs dipping more steeply than the eastern limbs (Al-Kaabi et al., 2023).

The thickness of the Zubair Formation varies across Iraq, increasing from approximately 200 m in the southwest near Saudi Arabia to about 500 m at the depocenter. Major oilfields, including the Zubair Oilfield, are situated within prominent north-south trending structural features southeast of the depocenter (Ali and Nasser, 1989).

4. Materials and Methods

This study utilized open-hole well log data from four different wells (Z1, Z2, Z3, and Z4) provided by Basrah Oil Company. The dataset includes key logs such as gamma-ray, self-potential, sonic, resistivity, density, and neutron logs (Table 1). These logs provide the foundation for analyzing and estimating the petrophysical properties of the Upper Shale Member and the Upper Sand Member of the Zubair Formation. Due to the unavailability of reliable density and neutron logs in some wells, the sonic log was employed to estimate total porosity (ØT).

A statistical analysis was performed in Minitab, with histograms and standard deviation curves created for shale volume (Vsh), total porosity, and hydrocarbon saturation. Initial calculations of essential petrophysical parameters and plotting were performed using Excel program. Subsequently, Techlog software was utilized for both qualitative and quantitative analyses, enabling the development of detailed petrophysical profiles for these members.

Table 1. Availability log data summary, including top and base depths, thickness, and RTKB for the four wells

Well No.	Dome	Log Data	Top (m)	Bottom (m)	Thickness (m)	RTKB (m)	
Z1	Hammar	✓	3187.6	3519.8	332.2	13.10	
Z2	Shuaiba	✓	3195.8	3521.8	326	27.02	
Z3	Rafidhya	✓	3231.4	3577.6	346.2	30.42	
Z4	Safwan	✓	3249.2	3558.8	309.6	16.03	
Well No.	Log Type						
	CAL	GR	NPHI	RHOB	ΔT	Rt	Rxo
Z1	✓	✓			✓	✓	✓
Z2	✓	✓	✓	✓	✓	✓	✓
Z3	✓	✓			✓	✓	✓
Z4		✓			✓	✓	✓

4.1. Calculation of Petrophysical Parameters

4.1.1. Shale volume (Vsh)

Calculating shale volume can be accomplished using various logs, including resistivity, spontaneous potential, gamma ray, and neutron logs. In the current study, the gamma-ray log was utilized (Asquith and Krygowski, 2004).

$$IGR = \frac{GR\ log - GR\ min}{GR\ max - GR\ min} \quad (1)$$

$$Vsh = (2^{(2*IGR)} - 1)/3 \quad (2)$$

Where: I_{GR}: Gamma-ray index, GR_{log}: Gamma-ray log reading (API), GR_{min}: Minimum gamma-ray log reading (clean sand) (API), GR_{max}: Maximum gamma-ray log reading (shale) (API), V_{sh}: Shale volume.

4.1.2. Porosity (Ø)

Porosity is essential for estimating a reservoir's capacity to store fluids, such as hydrocarbons and water. This study focuses on estimating various types of porosity: total porosity (ØN.D), effective porosity (ØE), primary porosity (ØS), and secondary porosity (SPI).

Total Porosity and Effective Porosity

The density and neutron logs are used to determine the total porosity; furthermore, necessary corrections based on shale volume and gamma-ray log readings are applied to calculate the effective porosity (Wyllie et al., 1958; Schlumberger, 1997; Darlling, 2005).

$$\emptyset D = \frac{\rho\, ma - \rho\, b}{\rho\, ma - \rho\, f} \quad (3)$$

$$\emptyset N.D = \frac{\emptyset N + \emptyset D}{2} \quad (4)$$

$$\emptyset N.Dc = \emptyset N.D * (1 - Vsh) \quad (5)$$

Where: ØD: Porosity derived from the density log. ρma: Density of the matrix (2.65g/cm^3). ρb: Density of the bulk formation (log reading) (g/cm^3). ρf: Density of the fluid (1 or 1.1g/cm^3). ØN.D: Total porosity derived from neutron and density logs. N: Porosity derived from the neutron log. ØN.Dc: Effective porosity (Shale-corrected porosity) derived from the neutron and density logs.

Primary Porosity and Secondary Porosity

To further refine the porosity analysis, sonic logs are used to calculate the primary porosity, which, in turn, aids in determining the secondary porosity (Wyllie et al., 1958; Schlumberger, 1997).

$$\emptyset S = \frac{\Delta t\, log - \Delta t\, ma}{\Delta t\, f - \Delta t\, ma} \quad (6)$$

$$SPI = \emptyset N.D - \emptyset S \quad (7)$$

Where: ØS: Porosity derived from the sonic log. Δt_{log}: Interval transit time in the formation (log reading) (µsec/ft). Δt_{ma}: Interval transit time within the rock matrix (µsec/ft). Δt_f: Interval transit time within the formation fluid (µsec/ft). SPI: Secondary porosity index.

Table 2. Acoustic velocities and densities for different lithologies and fluids (Schlumberger, 1972; Asquith and Krygowski, 2004)

Lithology	ρma (g/cm^3)	Δtma (µsec/ft)
Sandstone	2.65	55.5
Freshwater filtrate	1.000	189
Saltwater filtrate	1.150	185

4.1.3. Water saturation (SW, and Sxo) and hydrocarbon saturation (Sh)

Water saturation estimates for both the invaded and uninvaded zones are obtained using resistivity logs. Hydrocarbon saturation is then calculated by subtracting the water saturation in the uninvaded zone from unity (Archie, 1944; Arps, 1964; Schlumberger, 1987; Asquith and Krygowski, 2004).

$$SW = \sqrt{(F\ *\ Rw)/Rt} \quad (8)$$

$$Sxo = \sqrt{(F * Rmf)/Rxo} \quad (9)$$

$$Sh = 1 - SW \quad (10)$$

$$F = \frac{a}{\emptyset^m} \quad (11)$$

$$Rmf\ @\ Tf = Rmf\ @\ Ts * \left(\frac{Ts + 6.77}{Tf + 6.77}\right) \quad (12)$$

$$Tf = (G.G * d) + Ts \quad (13)$$

$$G.G = \frac{BHT - Ts}{TD} \quad (14)$$

Where: Sw: Saturation of water in the uninvaded zone. F: Formation Factor. Rw: Resistivity of formation water (Ω·m). Rt: Resistivity of the uninvaded zone derived from resistivity logs (Ω·m). Sxo: Saturation of water saturation in the invaded zone. Rmf: Resistivity of mud filtrate (Ω·m). Rxo: Resistivity of the invaded zone derived from resistivity logs (Ω·m). Sh: Saturation of hydrocarbon. a: Tortuosity factor (0.81) for sandstone. m: Cementation factor (2) for sandstone. Tf: Temperature of the formation (F˚). G.G: Geothermal gradient (F˚/m). BHT: Temperature of the borehole (F˚). Ts: Temperature of the mean annual surface (F˚). d: Formation depth (m). TD: Total well depth (m). Rmf @ Tf: Resistivity of the drilling mud filtrate (Ω·m) at Tf (F˚). Rmf @ Ts: Resistivity of the drilling mud filtrate (Ω·m) at Ts (F˚).

4.1.4. Bulk volume of water (BVW, and BVxo) and bulk volume of hydrocarbons (BVh)

The bulk volume of water is calculated for both the invaded and uninvaded zones, along with the bulk volume of hydrocarbons, offering insights into the fluid distribution within the reservoir (Schlumberger, 1998).

$$BVW = SW * ØN.D \quad (15)$$

$$BVXO = Sxo * ØN.D \quad (16)$$

$$BVh = Sh * ØN.D \quad (17)$$

Where: BVW: Bulk volume of water in the uninvaded zone. BVxo: Bulk volume of water in the invaded zone. BVh: Bulk volume of hydrocarbon.

4.1.5. Movable oil saturation (MOS) and residual oil saturation (ROS)

Finally, movable and residual oil saturation is derived, enhancing the understanding of hydrocarbon mobility and recovery potential (Spain, 1992; Schlumberger, 1998).

$$MOS = Sxo - Sw \quad (18)$$

$$ROS = 1 - Sxo \quad (19)$$

Where: MOS: Movable oil saturation. ROS: Residual oil saturation.

4.2. Manual Corrections of Petrophysical Parameters

4.2.1. Correction 1: Excluding tight sand zones based on porosity classification

This correction addresses the overestimation of water and hydrocarbon saturation values in intervals containing tight sand. Saturation parameters, such as water saturation in both invaded and non-invaded zones, and hydrocarbon saturation are derived from resistivity log readings. However, resistivity tools cannot distinguish between high resistivity caused by the presence of hydrocarbons and that caused by lithological factors, such as compaction. To correct this, and based on the porosity classification (Table 3), a rule was applied:

If the total porosity value falls within the range of 0 to 0.05, it is considered negligible and manually set to 0. The following observations justify this decision:

Gamma ray readings are low in these zones, indicating the presence of sand. Resistivity readings are high, not because of hydrocarbons, but due to compaction. By eliminating porosity in these intervals, all associated saturation values (water and hydrocarbon) were also set to zero, preventing misinterpretation of these tight sand zones as productive reservoir sections.

4.2.2. Correction 2: Calculation of effective porosity

The effective porosity is defined as the porosity that remains after accounting for the volume of shale. In order to isolate the effective porosity, several steps were taken to remove the shale contribution from the total porosity.

1. Removal of Shale from Areas with (Gamma Ray > 70 API)

In areas where the gamma ray reading exceeds 70 API, it is assumed that the formation consists primarily of shale. Therefore, the total porosity in these regions is set to zero. While the total porosity in shale-dominated zones is not strictly zero, this step serves to simplify the calculation by excluding shale from the porosity values for further processing.

2. Adjustment for Areas with Mixed Shale and Sand (Gamma Ray between 30 and 70 API)

In regions where the gamma ray reading falls between 30 and 70 API, a mix of shale and sand is present. To account for this, the total porosity values are adjusted by removing the shale contribution. The modified total porosity is calculated by multiplying the adjusted total porosity (after removing the pure shale regions) by the factor (1 − shale volume). This step effectively eliminates the shale component in the mixed zones, isolating the sand portion and providing an accurate estimate of the effective porosity.

3. Retention of Porosity in Clean Sand Zones (Gamma Ray < 30 API)

In areas where the gamma ray reading is less than 30 API, the formation is considered to consist almost entirely of clean sand with minimal to no shale content. These zones are assumed to represent effective porosity already; therefore, no further corrections are applied. This final step ensures that the clean sand intervals maintain their original porosity values, completing the process of isolating effective porosity across the entire formation.

Table 3. Porosity classification (Ganat, 2020)

Porosity	Type of Porosity
Negligible	0 - 5%
Poor	5 - 10%
Fair	10 - 15%
Good	15 - 20%
Very good	20 - 25%
Excellent	< 25%

5. Results and Discussion

In this study, histograms of shale volume, total porosity, and hydrocarbon saturation were first generated (Figs. 5, 6, and 7), which also provided standard deviation values to illustrate the variability of these parameters. Following this, average values of total porosity, effective porosity, bulk volume hydrocarbon (BVH), and effective bulk volume hydrocarbon (EBVH) were calculated per member for each well (Figs. 8, 9, 10, and 11) to simplify interpretation and highlight overall reservoir trends. BVH and EBVH were derived by multiplying total and effective porosities by hydrocarbon saturation. Before this, porosity values corresponding to gamma ray readings above 70 API and those below 0.05 were excluded due to their association with non-productive zones. Additionally, hydrocarbon saturation values below 0.30 were excluded to ensure only productive zones were considered.

All four studied wells also showed indications of heavy, tar-like hydrocarbons. Similar accumulations, known as tar mats, were reported in the Main Pay of the Zubair Formation in the North Rumaila Oilfield by Jawad and Handhal (2019), suggesting that the presence of such heavy hydrocarbons may represent a regional feature of the formation.

The following sections provide a detailed description and highlight productivity trends based on BVH and EBVH values.

1. Upper Shale Member (Z/1)

The Upper Shale Member, also known as the (Z/1) member, is primarily composed of shale with interbedded sandstone units and consists of five units: Ushale 5, Ushale 4, Ushale 3, Ushale 2, and Ushale 1, arranged in stratigraphic order from top to bottom. Based on BVH and EBVH values, the most productive well in this member is (Z1) at Hammar Dome, while the least productive is (Z3) at Shuaiba Dome and (Z4) at Safwan Dome (Table 4).

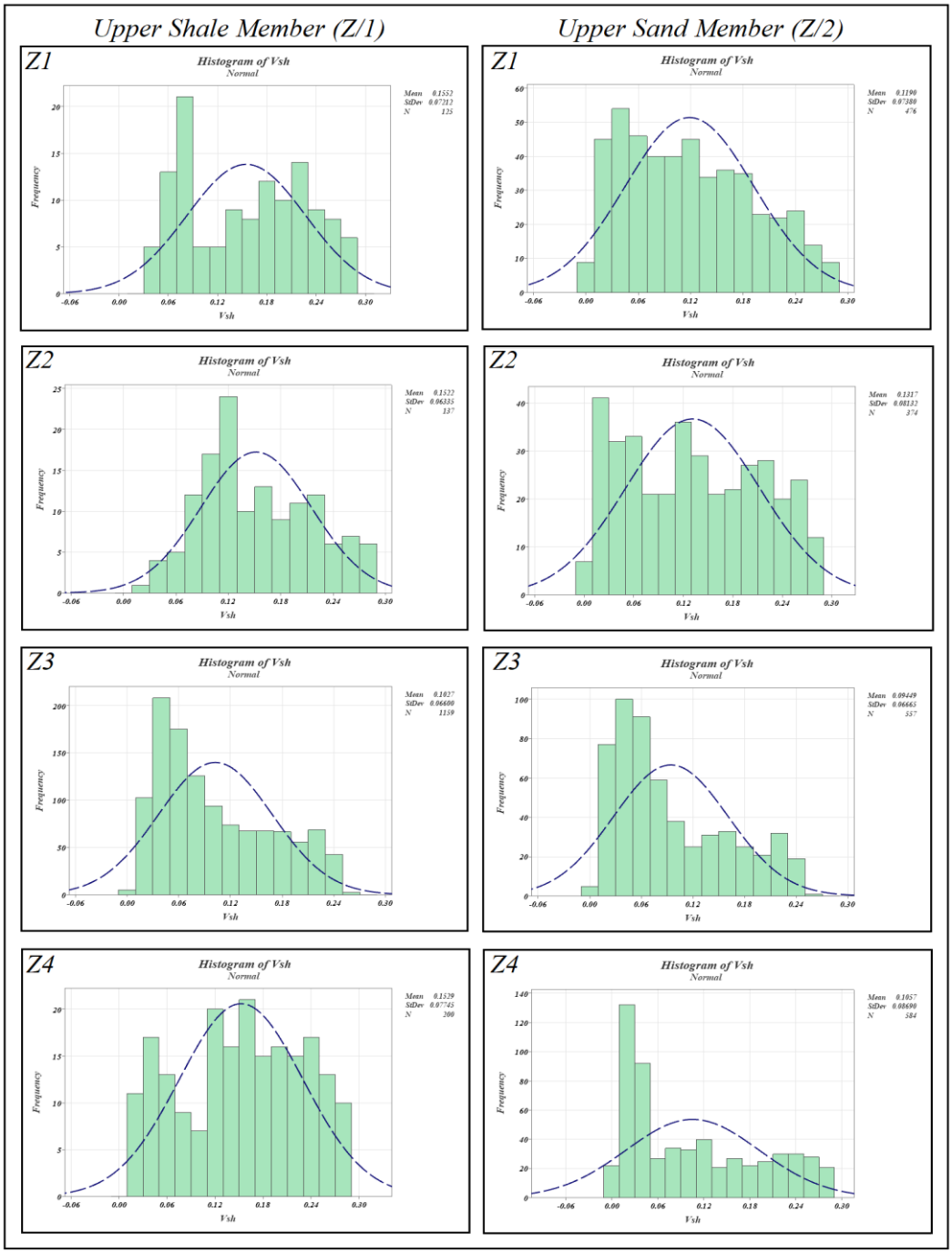


Fig. 5. Histogram and standard deviation of shale volume for Upper Shale Member (Z/1) and Upper Sand Member (Z/2) in wells Z1, Z2, Z3, and Z4

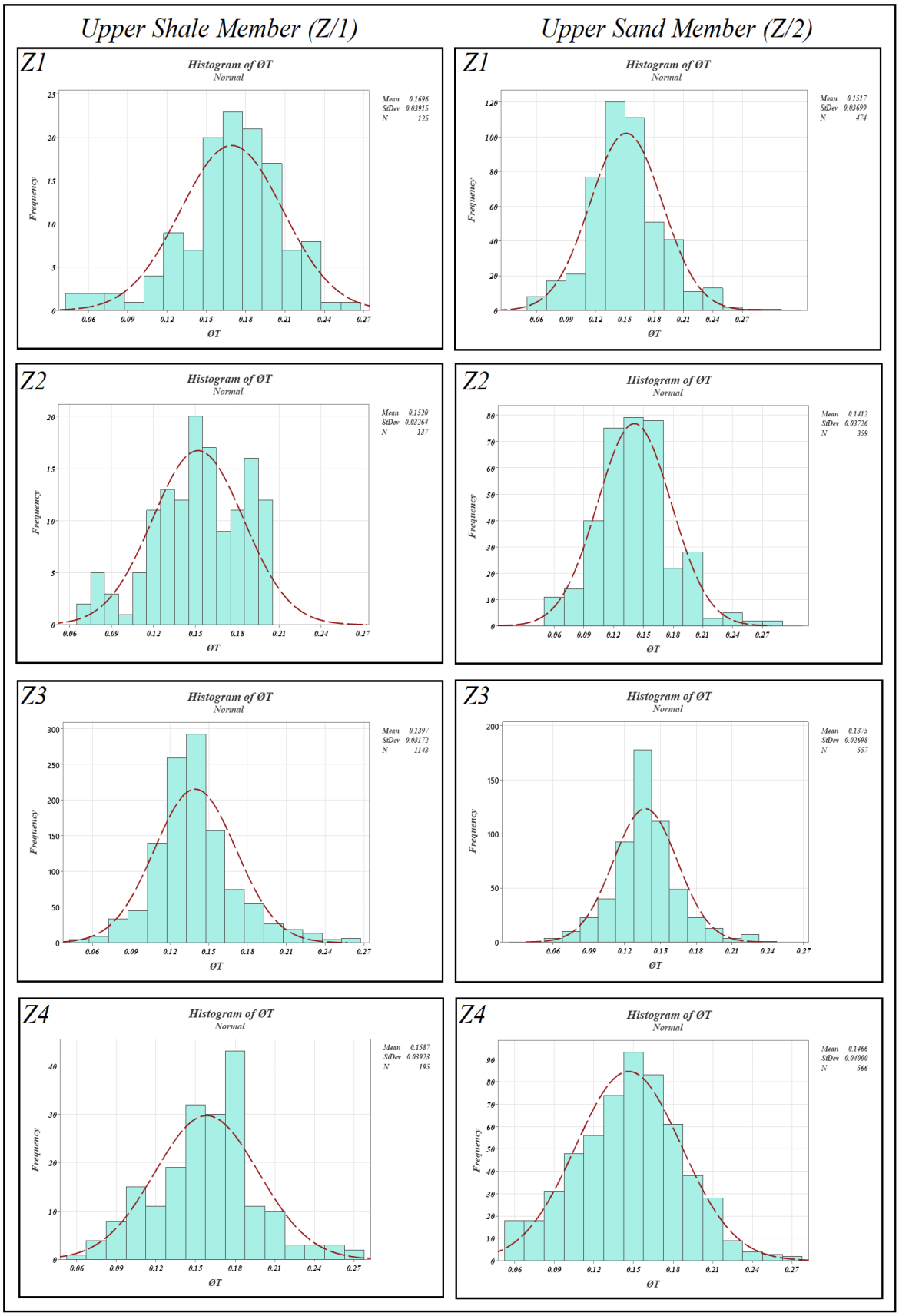


Fig. 6. Histogram and standard deviation of total porosity for Upper Shale Member (Z/1) and Upper Sand Member (Z/2) in wells Z1, Z2, Z3, and Z4

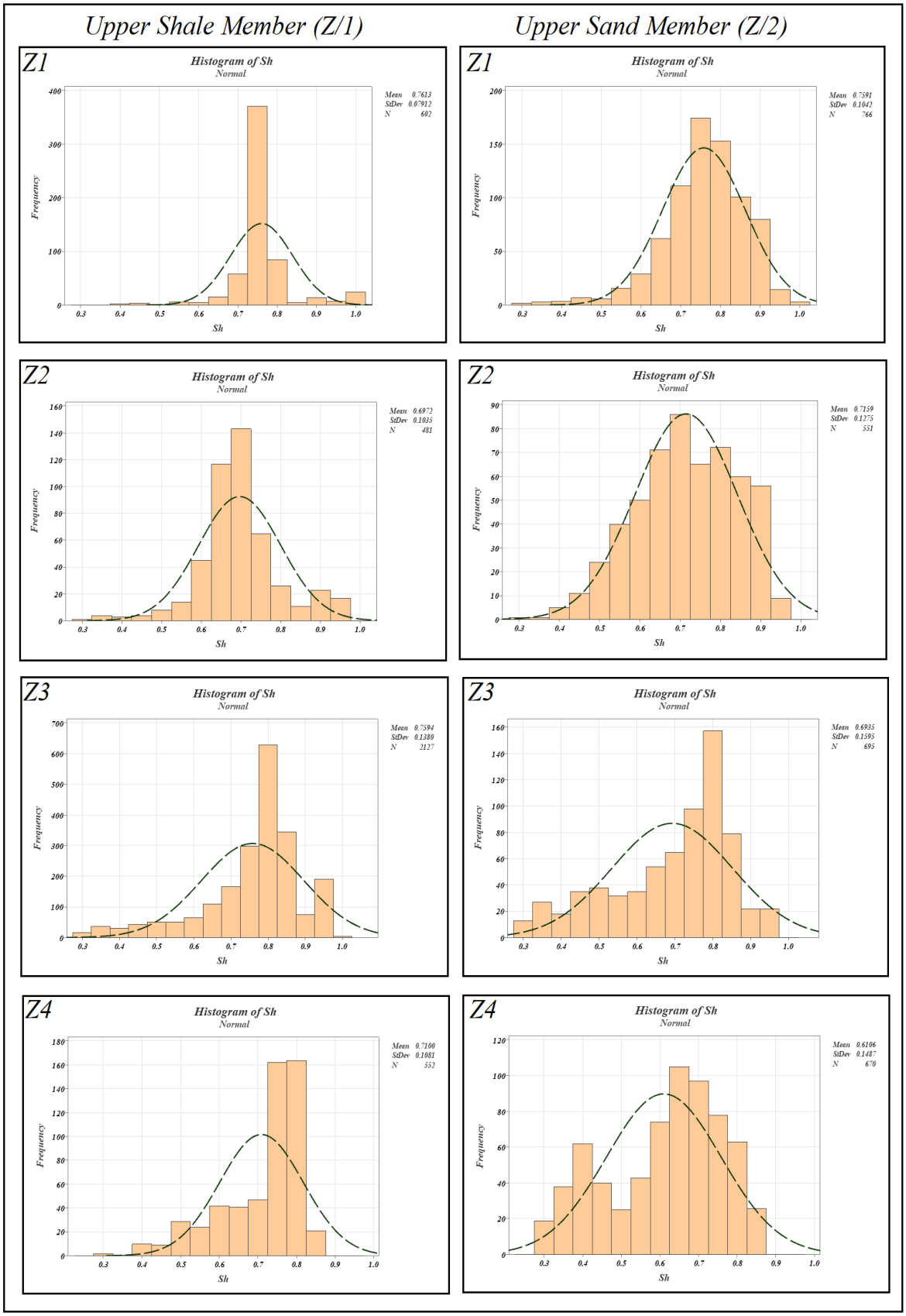


Fig. 7. Histogram and standard deviation of hydrocarbon saturation for Upper Shale Member (Z/1) and Upper Sand Member (Z/2) in wells Z1, Z2, Z3, and Z4

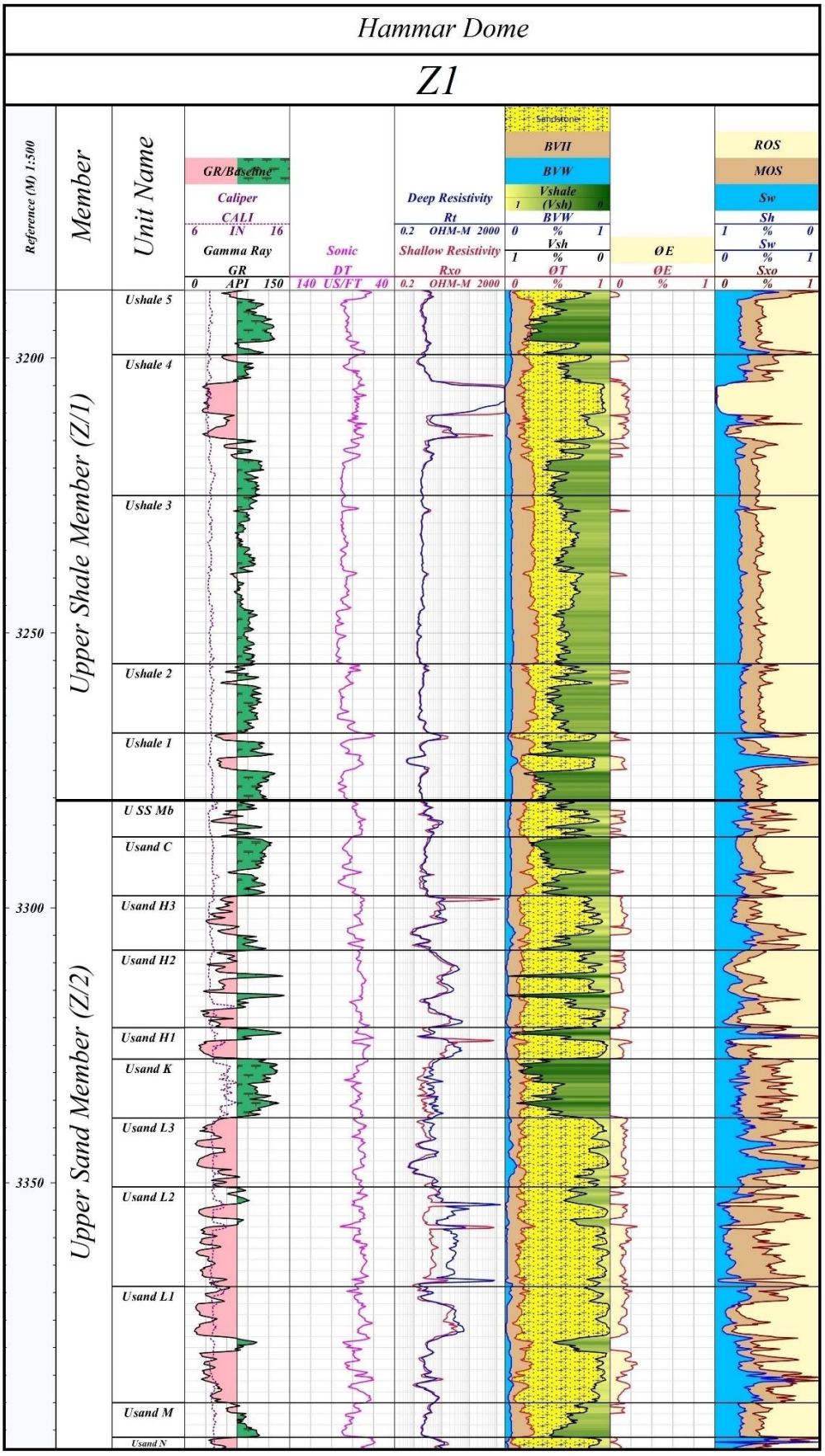


Fig. 8. Qualitative and quantitative petrophysical interpretation for Z1

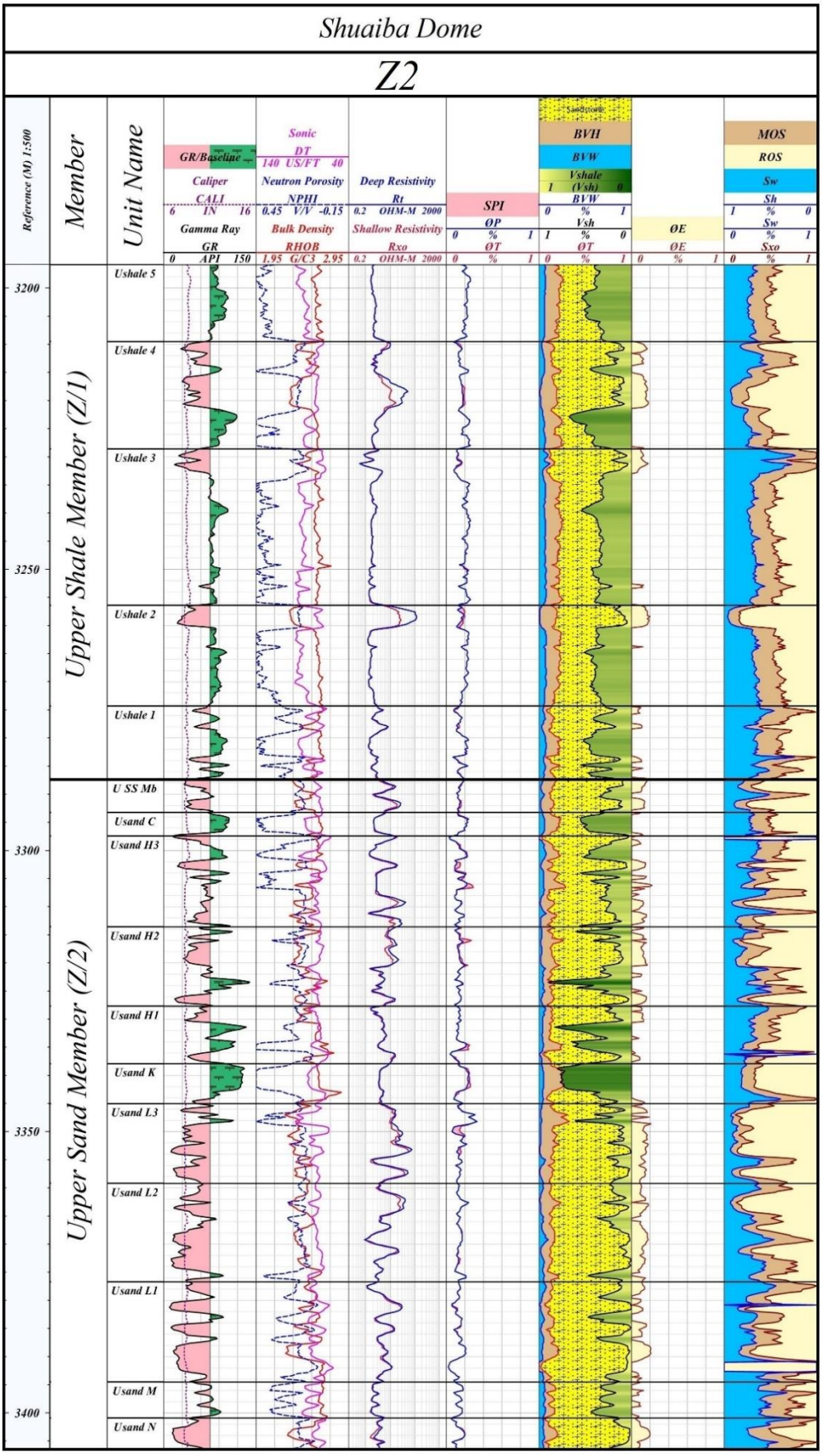


Fig. 9. Qualitative and quantitative petrophysical interpretation for Z2

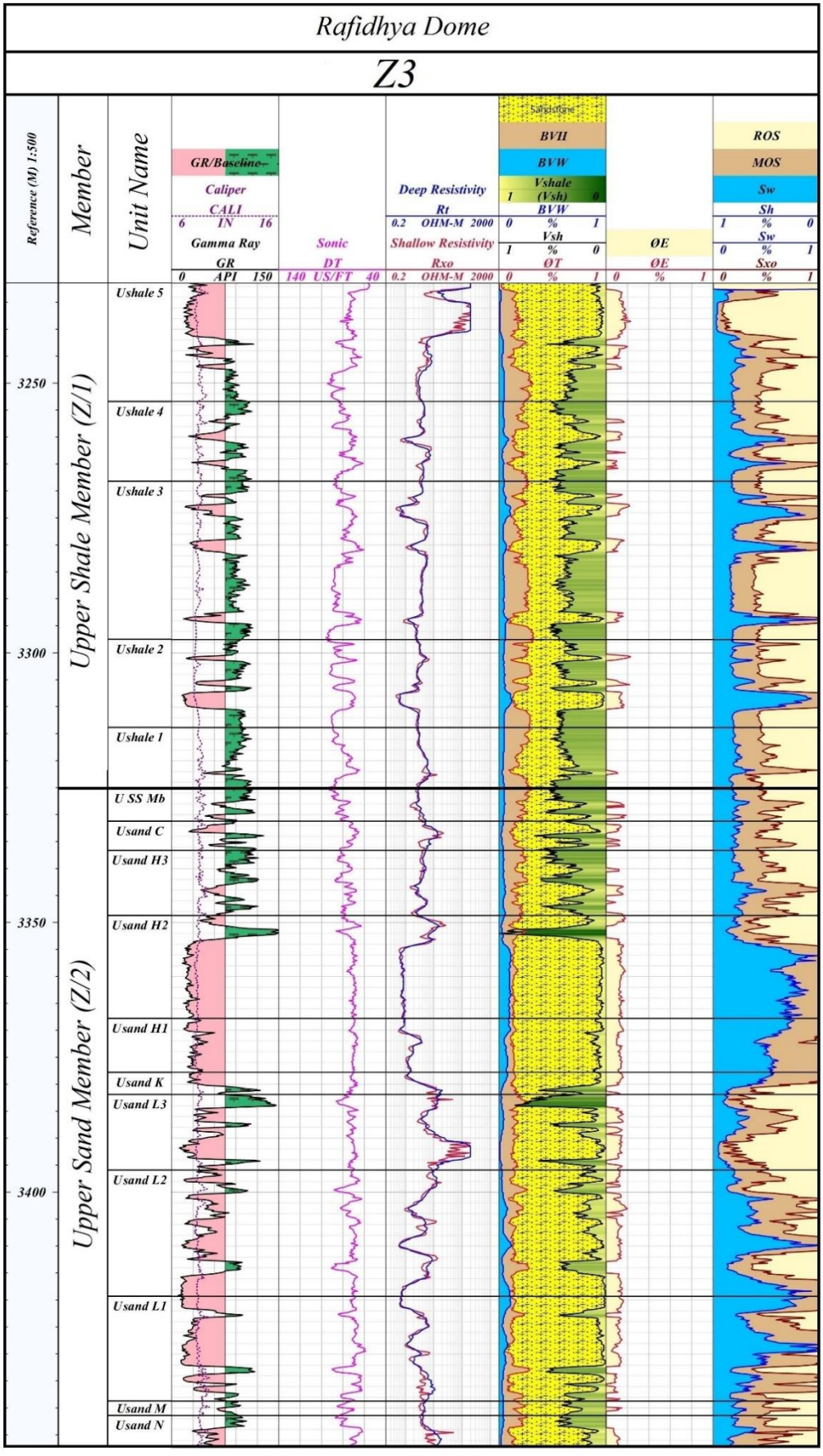


Fig. 10. Qualitative and quantitative petrophysical interpretation for Z3

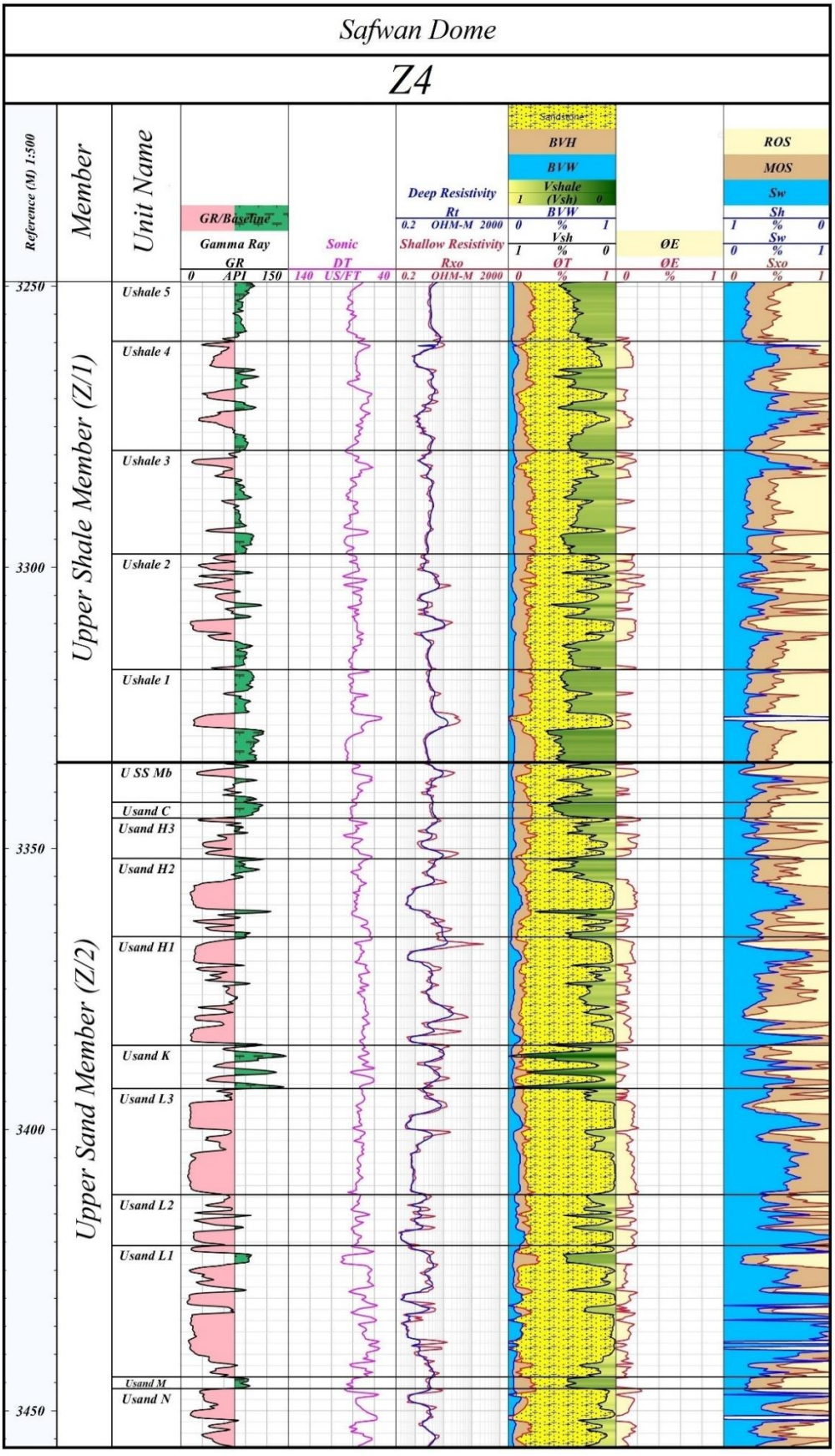


Fig. 11. Qualitative and quantitative petrophysical interpretation for Z4

4. Upper Sand Member (Z/2)

The Upper Sand Member, or (Z/2) member, consists mainly of sandstone with some shale interbeds and includes eleven units: U SS Mb, Usand C, Usand H3, Usand H2, Usand H1, Usand K, Usand L3, Usand L2, Usand L1, Usand M, and Usand N, also presented in stratigraphic order from top to bottom. Among the available data, the highest BVH and EBVH values are recorded at (Z1) in Hammar Dome, while the lowest values are found in (Z4) at Safwan Dome (Table 4).

Table 4. Average petrophysical properties of the Upper Shale Member and the Upper Sand Member of Zubair Formation

	Upper Shale Member (Z/1)				
	Well No.	Z1	Z2	Z3	Z4
	Dome	Hammar	Shuaiba	Rafidhya	Safwan
	Depth (m)	3187.6-3280.5	3195.8-3287.4	3231.4-3325.2	3249.2-3334.7
	Thickness (m)	92.9	91.6	93.8	85.5
Average (%)	Vsh	0.41	0.34	0.29	0.32
	ØT	0.17	0.15	0.15	0.16
	ØE	0.14	0.13	0.14	0.14
	SH	0.76	0.69	0.77	0.71
	Sxo	0.43	0.39	0.53	0.58
	MOS	0.19	0.08	0.30	0.29
	BVH	0.13	0.10	0.12	0.11
	EBVH	0.11	0.09	0.11	0.10
	Upper Sand Member (Z/2)				
	Well No.	Z1	Z2	Z3	Z4
	Dome	Hammar	Shuaiba	Rafidhya	Safwan
	Depth (m)	3280.5-3398.5	3287.4-3406.7	3325.2-3447.4	3334.7-3456.4
	Thickness (m)	118	119.3	122.2	121.7
Average (%)	Vsh	0.27	0.24	0.20	0.19
	ØT	0.15	0.14	0.14	0.15
	ØE	0.13	0.12	0.13	0.13
	SH	0.76	0.72	0.69	0.61
	Sxo	0.52	0.35	0.71	0.74
	MOS	0.28	0.07	0.40	0.35
	BVH	0.11	0.10	0.10	0.09
	EBVH	0.10	0.09	0.09	0.08

Each profile consists of two main sections: the raw well log data and the calculated interpretations. The original logs, such as gamma-ray, sonic, caliper, and resistivity, were provided by the Basra Oil Company for academic purposes. All quantitative interpretations, including Vsh, total and effective porosity (ØT, and ØE), Sw, Sh, BVW, BVH, saturation in the invaded zone (Sxo), movable oil saturation (MOS), and residual oil saturation (ROS), were independently carried out by the author.

Only well Z2 (Shuaiba Dome) contains density–neutron logs; the remaining wells lack these logs due to data limitations from the Basra Oil Company, which also relies on sonic logs for porosity estimation in this clastic formation. In well Z2, porosity values derived from both the sonic and the density–neutron logs were nearly identical (Fig. 9), confirming the reliability of sonic logs for total porosity estimation. Additionally, statistical analysis of total porosity distributions across all wells (Fig.6) revealed near-normal patterns with minimal skewness, indicating homogeneity and supporting the consistent use of sonic logs throughout the dataset.

6. Conclusions

This study presents a petrophysical evaluation of the Upper Shale Member (Z/1) and the Upper Sand Member (Z/2) of the Zubair Formation, located in the Zubair Oilfield in southern Iraq. The field comprises four main structural domes: Hammar, Shuaiba, Rafidhiya, and Safwan. One well was selected from each dome for detailed analysis: Z1 (Hammar Dome), Z2 (Shuaiba Dome), Z3 (Rafidhiya Dome), and Z4 (Safwan Dome).

The research involved both qualitative and quantitative petrophysical interpretations of these two upper members, which are part of the five main members of the Zubair Formation. The results indicate that the best petrophysical properties in both the Upper Shale Member and the Upper Sand Member were observed in the Hammar Dome (Z1). In contrast, the poorest petrophysical quality in the Upper Shale Member was observed in the Shuaiba Dome (Z2), whereas in the Upper Sand Member it was found in the Safwan Dome (Z4). This conclusion is supported by a table summarizing average values of shale volume (Vsh), total and effective porosity (ØT, ØE), bulk volume hydrocarbon (BVH), effective bulk volume hydrocarbon (EBVH), movable oil saturation (MOS), and water saturation in the invaded zone (Sxo). Petrophysical quality was assessed primarily through the averages of BVH and EBVH, which reflect the reservoir's hydrocarbon storage capacity and potential deliverability.

Acknowledgments

I would like to thank Prof. Dr. Fahad Mansour Al-Najm for his guidance, and Assist. Prof. Dr. Bassim Hameed Sultan for his support during this research. I also appreciate the assistance of Lecturer Hiba Ahmed Al-Samer. Thanks are extended to the Department of Geology at the University of Basra for their continued support.

References

Abdulnaby, W., 2018. Structural geology and neotectonics of Iraq, Northwest Zagros. PhD thesis, University of Basra. https://doi.org/10.1016/B978-0-12-815048-1.00004-4

Alher, A., Al-Jawad, M.S., Al-Yasery, A., 2018. Static model of Zubair reservoir in Luhais oilfield. Iraqi Journal of Chemical and Petroleum Engineering, 19(1), 57–60. https://doi.org/10.31699/IJCPE.2018.1.7

Ali, A.J., Nasser, M.E., 1989. Facies analysis of the Lower Cretaceous oil-bearing Zubair Formation in southern Iraq. Modern Geology, 13(3–4), 225–242.

Al-Kaabi, M., Hantoosh, D., Neamah, B., Almohy, H., Bahlee, Z., Mahdi, M. and Abdulnaby, W., 2023. Classification of the Zubair subzone oilfields using structural contour maps, southern Iraq. Journal of African Earth Sciences, 197, 104770. https://doi.org/10.1016/j.jafrearsci.2022.104770

Al-Mutury, W.G., Al-Mayahi, D.S.B., 2010. Geometric and genetic structural analysis of Zubair oilfield, southern Iraq. Qadissya for Sciences, 3, 89–97.

Al-Najar, A.M.S., 1989. Using of paleomagnetism to determine the recent sediment in the south of Iraq. MSc. thesis. Baghdad University. (In Arabic).

Al-Samer, H.A.H., Al-Najm, F.M., 2024. Petrophysical and statistical analysis of main pay of the Zubair Formation in South Rumaila Oil Field. Iraqi Journal of Science, 65(1), 210-222. https://doi.org/10.24996/ijs.2024.65.1.19

Archie, G.E., 1944. The electrical resistivity log as an aid in determining some reservoir characteristics. Petroleum Technology, 5, 54–62. https://doi.org/10.2118/942054-G

Arps, J.J., 1964. Engineering concepts useful in oil finding. AAPG Bulletin, 48, 157–165. https://doi.org/10.1306/BC743BD9-16BE-11D7-8645000102C1865D

Asquith, G.B., Krygowski, D., 2004. Basic Well Log Analysis (2nd ed.). AAPG Methods in Exploration Series, no. 16. The American Association of Petroleum Geologists.

Buday, T., Jassim, S., 1987. The regional geology of Iraq: Tectonics, magmatism, and metamorphism. In: Kassab, I.I., Abbas, M.J. (Eds.), Geology of Iraq. Geologic Survey, Baghdad.

Darling, T., 2005. Well Logging and Formation Evaluation. Gulf Professional Publishing.

Ganat, T.A.O., 2020. Fundamentals of Reservoir Rock Properties. Springer International Publishing.

Jassim, S.Z., Goff, J.C., 2006. The Geology of Iraq. Dolin Publishing, Czech Republic.

Jawad, S.M., Handhal, A.M., 2019. Identification of heavy oil (tar mats) deposits and forming mechanism in the main pay of the Zubair Formation in North Rumaila Oil Field, Southern Iraq. International Journal of Mining Science, 5(1), 1–10. https://doi.org/10.20431/2454-9460.0501001

Mahdi, T.A., Mustafa, J., 2018. Facies modeling of the Mishrif Formation in selected wells of the Tuba oilfield, southern Iraq. International Journal of Advanced Engineering Research and Science, 5(1), 22–29. https://doi.org/10.22161/ijaers.5.1.5

Numan, N.M.S., 2000. Major Cretaceous tectonic events in Iraq. Rafidain Journal of Science, 11(3), 32–52.

Powers, R.W., Ramirez, L.F., Redmond, C.D., Elberg, E.L. Jr., 1966. Sedimentary Geology of Saudi Arabia: Geology of the Arabian Peninsula. U.S. Geological Survey Professional Paper No. 560D, U.S. Geological Survey, Washington, DC.

S.O.C., 1986. Structural map of upper part of Zubair Formation. Report no. 134. Basrah, Iraq.

Schlumberger, 1972. Log Interpretation Manual: Principles. Vol. I. Schlumberger Well Services Inc.

Schlumberger, 1987. Log Interpretation Charts. Schlumberger Wireline.

Schlumberger, 1997. Log Interpretation Charts. Schlumberger Wireline.

Schlumberger, 1998. Log Interpretation Principles/Applications (17th printing). Schlumberger Wireline & Testing.

Spain, D.R., 1992. Petrophysical evaluation of a slope fan/basin floor fan complex: Cherry Canyon Formation, Ward County. AAPG Bulletin, 76(6), 805–827. https://doi.org/10.1306/BDFF88E4-1718-11D7-8645000102C1865D

Wyllie, M.R.J., Gregory, A.R., Gardner, G.H.F., 1958. An experimental investigation of the factors affecting elastic wave velocities in porous media. Geophysics, 23(4), 459–493. https://doi.org/10.1190/1.1438493